Chemistry–A European Journal
Concept
doi.org/10.1002/chem.202303345
Chemistry Europe
European Chemical Societies Publishing
www.chemeurj.org

Electronic Modulation in Homonuclear Dual-Atomic Catalysts for Enhanced CO_2 Electroreduction

Wen-Jie Shi,[a] Yu-Chen Wang,[a] Wei-Xue Tao,[a] Di-Chang Zhong,*[a] and Tong-Bu Lu*[a]

Homonuclear dual-atomic catalysts showcase unique electronic modulation due to their dual metal centres, providing new direction in development of efficient catalysts for CO_2 electroreduction. This article highlights a few cutting-edge homonuclear dual-atomic catalysts, focusing on their inherent advantages in efficient and selective CO_2 electroreduction, to spotlight the potential application of dual-atomic catalysts in CO_2 electroreduction.

Introduction

In the context of accelerating global industrialization and burgeoning populations, the nexus of energy demand and ecological sustainability presents pressing challenges.[1] Foremost among these is the pursuit of sustainable energy solutions. Electrocatalytic CO_2 reduction reaction (CO_2RR) emerges as a beacon, providing a promising approach to address rising energy demands while exemplify environmental stewardship.[2] Therefore, the exploration of CO_2RR electrocatalysts with low cost and energy input as well as high Faraday efficiency (FE) and product selectivity is urgently demanded. Single-atom catalysts (SACs) has significantly shifted the paradigm in electrocatalytic CO_2RR research.[3] While the high atomic efficiency and robust catalytic activity of SACs have spurred extensive studies, their inherent structural simplicity occasionally acts as a double-edged sword. The absence of neighboring active sites can become a hindrance in more intricate electrocatalytic reactions. This is why dual-atomic catalysts (DACs) come into the picture of CO_2RR.[4] Featured by their binary metal sites, DACs not only hold promise in addressing the limitations of SACs but also introduce a novel dimension of catalysis, like modulate both electronic configuration of the catalytic centers and geometric structure of the catalysts. Their distinct advantage lies in the synergistic interplay between the two metal atoms, which can enhance catalytic activities in CO_2RR.[5]

The efficacy of electrocatalysts is intrinsically tied to the electronic structure of their catalytic sites. Precise adjustments to the structure can significantly reduce the energy barriers for key intermediate formation, thereby refining catalytic performance.[6] A slew of modern strategies focus on modulating the electronic structures of catalytic sites to optimize efficiency. Notably, modifying the coordination environment of a single-metal center in SACs has been impactful,[7] due to the seamless electron transfer between metal centers and their coordinating atoms. Given this precedent, adjusting the electron configuration of the dual-metal centers in DACs can be a logical evolution, potentially bolstering electrocatalytic activities for CO_2RR.

Homonuclear dual-atomic-site catalysts (HDACs) is a subset of DACs, which introduce a new approach for electrocatalytic CO_2 reduction (Scheme 1).[8] While DACs have been recognized for their synergistic properties stemming from adjacent metal atoms, HDACs with two identical metal atoms, provide not just a synergistic boost, but a mode for diverse electronic configurations. This characteristic of HDACs positions them as promising entities for future research in the realm of electrocatalytic CO_2RR.[8–9] In this concept, based on recent works by us and others in the subject, we address the current understanding of modulating electron configuration of catalytic centers in HDACs, and casting a vision for their potential in electrocatalytic CO_2RR.

1. Optimization of Electronic Structure by Intermetallic Direct Interaction

In contrast to SACs, HDACs presented the synergistic effect between adjacent metal atoms, which promote their catalytic activity while maintaining the advantages of SACs, like 100%

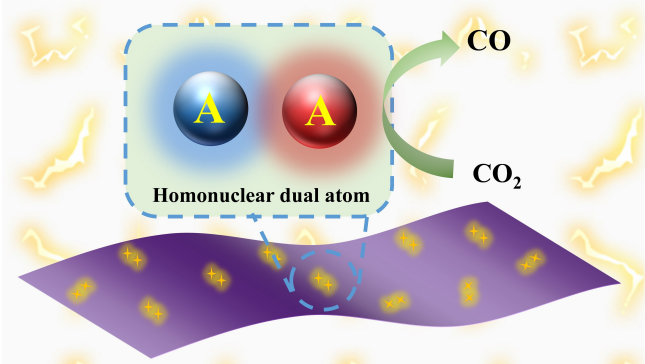

Scheme 1. Scheme of the HDACs for electrocatalytic CO_2RR.

[a] *Prof. W.-J. Shi, Y.-C. Wang, W.-X. Tao, Prof. D.-C. Zhong, Prof. T.-B. Lu*
Institute for New Energy Materials & Low Carbon Technologies
School of Material Science & Engineering
Tianjin University of Technology
Tianjin 300384 (China)
E-mail: zhong_dichang@hotmail.com
lutongbu@tjut.edu.cn

atomic utilization efficiency and excellent selectivity.[10] Li et al. firstly used anion replacement deposition-precipitation method to prepare a novel acetylene black supported Pd_2 HDAC, further applied it for CO_2RR for the first time (Figure 1a).[11] Pd_2 HDAC demonstrated exceptional electrocatalytic efficiency in CO_2RR. The FE_{CO} was consistently above 80% in the potentials from −0.7 to −0.95 V, and the highest selectivity toward CO with maximum FE_{CO} reached 98.2% at −0.85 V vs. RHE (Figure 1b), outperforming the Pd_1 SAC counterpart. DFT insights revealed that this Pd_2 HDAC had an optimal potential determining step (PDS) free energy barrier of 1.28 eV, which is lower than that on Pd_1 SAC (1.86 eV), accounting for its superior electrocatalytic CO_2RR activity. In the *CO adsorption state, there are more electrons that can be transferred to CO* on Pd_2 (0.22e) compared to that on Pd_1 (0.04e), presented the electron transfer between two Pd atoms at the dimeric Pd_2 active sites (0.39e from $Pd_{2\#}$ to $Pd_{1\#}$; Figure 1c). This high efficiency also stems from the harmonious interaction between the Pd_2 dual atoms and their substrate, facilitating the electron transfer and enhancing the Pd active center binding to CO_2RR intermediates.

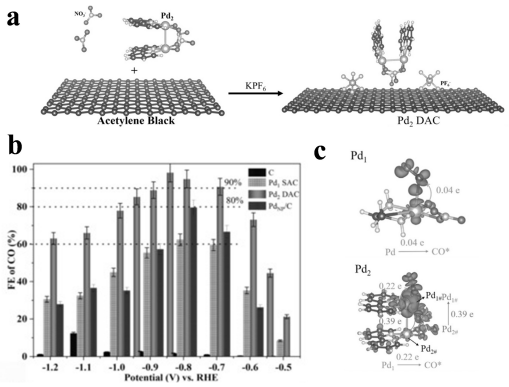

Figure 1. (a) The preparation strategy for Pd_2 HDAC. (b) FE_{CO} of C, Pd_{NP}/C, Pd_1 SAC, and Pd_2 HDAC in CO_2-saturated 0.5 M $KHCO_3$ electrolyte. (c) Charge density differences for CO* adsorption states and corresponding charge transfer on the Pd_1 and Pd_2 models. Reprinted with permission from Ref. [11] Copyright 2021, John Wiley and Sons.

2. Optimization of Electronic Structure by Intermetallic Indirect Interaction

Beside the direct interactions between two close dual metals, the indirect interactions of two dual metals will also tune the electron configuration in DACs, boosting the electrocatalytic activity in CO_2 reduction. Yao et al. developed a nitrogen-doped

Prof. Wen-Jie Shi serves as an Associate Professor in New Energy Materials & Low Carbon Technologies at Tianjin University of Technology. She obtained her B.S. in Chemistry from Gannan Normal University in 2015 and her PhD in Inorganic Chemistry from Xiamen University, respectively. Her interests focus on the rational design and synthesis of functional heterogeneous catalysts for energy storage and conversion.

Ms. Yu-Chen Wang received her B.S. in Liaocheng University in 2019 and M.S. in Tianjin University of Technology in 2022. Respectively. She is currently a PhD student at Tianjin University of Technology under the supervision of Prof. D. C. Zhong. Her current research is focused on the design and synthesis of functional complexes for energy storage and conversion.

Mr. Wei-Xue Tao obtained his BS degree from Tianjin University of Technology in 2019. He is currently a M.S. student at the same university under the supervision of Dr. W. J. Shi. His current research focuses on the design and synthesis of functional heterogeneous catalysts for energy storage and conversion.

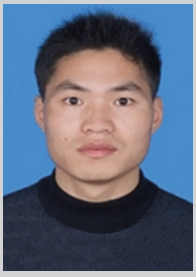

Prof. Di-Chang Zhong obtained his BS in 2003 from Gannan Normal University and his MS in 2006 from Guangxi Normal University and PhD in 2011 from the Sun Yat-Sen University. Then, he joined the faculty at Gannan Normal University and was promoted as Professor in 2017. He worked as a JSPS Post Doctoral Fellow at AIST, Japan for two years. In 2020, he moved to Tianjin University of Technology. His interests focus on the design and synthesis of molecular catalytic materials for energy storage and conversion.

Prof. Tong-Bu Lu obtained his BS in 1988 and PhD in 1993 from Lanzhou University. After two years post-doctoral fellowship at Sun Yat-Sen University, he joined the faculty at the same university, and became a professor in 2000. He worked as a post-doctoral fellow in F. Albert Cotton's group at Texas A&M University in 1998 and 2002, respectively. In 2016, he moved to Tianjin University of Technology. His current research interests focus on the study of artificial photosynthesis, including the design of homogeneous and heterogeneous catalysts for water splitting and CO_2 reduction.

carbon supported dinuclear Ni_2 catalyst (Ni_2/NC) by pyrolysis of a Ni_2 cluster and ZIF-8.[12] The high-magnification high-angle annular dark-field scanning transmission electron microscopy (HAADF-STEM) images of Ni_2/NC revealed an inter-nickel distance of roughly 2.9 Å. In electrocatalytic assessments, Ni_2/NC exhibited a FE_{CO} of 94.3% at a current density of 150 mA cm^{-2}, notably outperforming Ni_1/NC and NC catalysts by approximately 1.3 and 10.6 times, respectively (Figure 2a). During operando XAFS measurements under open-circuit voltage (OCV) conditions, a slight energy shift was observed in the absorption edge of Ni in Ni_2/NC, hinting at an elevated Ni oxidation state. This phenomenon may arise from the adsorption of specific oxo-species in the solution, optimizing the structure with a higher valence Ni (Figure 2b). Additionally, the extended X-ray absorption fine structure (EXAFS) examined the Ni–O configuration in Ni_2/NC under OCV approximating. Expanding upon these findings, the authors postulated an O–Ni_2–N_6 configuration. This O bridge led to a 0.2 Å contraction in the distance between adjacent Ni atoms compared to the initial Ni_2–N_6 structure, indicating the stronger Ni–Ni interactions. Integrated crystal orbital Hamilton population (ICOHP) were calculated to be −2.20 and −2.01 eV for the O–Ni_2–N_6 and Ni–N_4, further affirmed the optimized bonding and antibonding orbital populations in the O–Ni_2–N_6 model. Bader charge analysis provided deeper insights into charge populations and transfer dynamics, revealing that the O–Ni_2–N_6 possessed the highest positive charge of 0.23e, underscoring its superior efficiency in the activation of CO_2 to COOH* within the homonuclear Ni_2 active sites (Figure 2c).

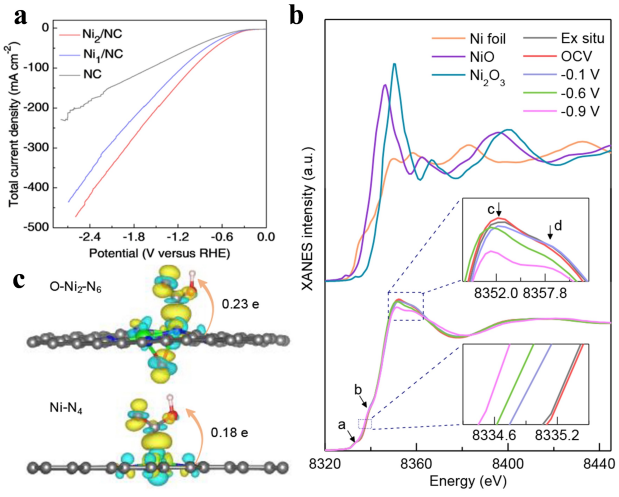

Figure 2. (a) LSV curves in the CO_2-flowed 1.0 M $KHCO_3$ electrolytes for the Ni_2/NC, Ni_1/NC, and NC catalysts. (b) Operando XANES spectra recorded at the Ni K-edge of Ni_2 HDAC, at different applied potentials from the OCV to −0.9 V during the electrocatalytic CO_2RR, and the XANES data of the referenced standards of NiO, Ni_2O_3, and Ni foil. Inset: Magnified absorption edge and white-line peak of XANES region. (c) Electron density difference plot of the *COOH intermediate adsorption structure on O–Ni_2–N_6 and Ni–N_4 and the Bader charge analysis. The isosurface value was set to be 0.003 electrons $Bohr^{-3}$. Yellow and cyan contours stand for the electron accumulation and deletion, respectively. Reprinted with permission from Ref. [12] Copyright 2021, American Chemical Society.

3. Optimization of Electronic Structure by Coordination Environment Modulation

Previous literature demonstrates that modulating the coordination environment of single-metal centers within SACs effectively alters their electronic structures.[13] This alteration stems primarily from the direct electron transfer between metal centers and coordinating atoms. For instance, the non-noble Fe SACs exhibit low overpotentials for CO_2 reduction to CO.[14] However, the robust adsorption of *CO intermediate at Fe-N–C sites constrains the CO desorption, leading to attenuated reaction kinetics. Han et al. reported a well-defined dual-atomic Fe_2 anchored on a nitrogen-doped carbon matrix synthesized through the pyrolysis of Fe-ZIF-8.[15] The resulted Fe_2 HDAC showed FE_{CO} exceeding 80% over broader potential ranges, coupled with a higher turnover frequency (26,637 h^{-1}) and superior durability compared to conventional Fe SAC analogs (Figure 3a). The morphology of Fe_2 HDAC retains the characteristics of Fe-ZIF-8, averaging around 150 nm in size. Atomic-resolution HAADF-STEM analysis confirmed bimetallic Fe sites rather than mere Fe clusters on the substrate (Figure 3b). Statistical analysis presented the bimetallic sites with a typically average distance of 2.37 ± 0.31 Å (Figure 3c). X-ray absorption fine-structure (XAFS) studies differentiated Fe SAC and Fe_2 HDAC configurations, with Fe_2–N_6–C-*o* showcasing superior CO_2RR catalytic activity. DFT calculations, as well as the CO_2 and CO temperature-programmed desorption (TPD) experiments highlighted the variations in CO_2 and *CO adsorption between Fe–N–C and Fe_2-N_6-C structures. Especially noting the minimal charge transfer between Fe and the CO intermediate on the Fe_2–N_6–C-*o* structure (Figure 3d). Due to electron delocalization caused by the Fe-3d orbital coupling of Fe_2–N_6–C-*o*, the energy gap between antibonding and bonding states was much smaller in Fe_2–N_6–C-*o* than Fe_1–N_4–C (Figure 3e), indicating a

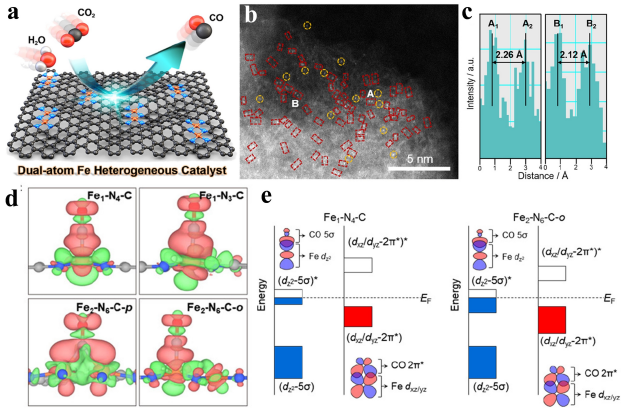

Figure 3. (a) Scheme of Fe_2–N_6–C-*o* HDAC. (b) Aberration-corrected (AC)-HAADF-STEM image of Fe_2–N6–C-*o*, in which single sites and bimetallic Fe pairs were highlighted by yellow circles and red rectangles. (c) Intensity profiles obtained on the two sites in areas A and B in Figure b. (d) Charge density difference of *CO adsorption with an isosurface level of 0.002 e·Å^{-3}. (e) Schematic illustration of orbital interaction between Fe-3d (dz^2 and d_{xz}/d_{yz}) and adsorbed CO (5σ and 2π*) for Fe_1–N_4–C and Fe_2–N_6–C-*o*. Reprinted with permission from Ref. [15] Copyright 2022, American Chemical Society.

weaker Fe–C bond and easier *CO adsorption in Fe_2–N_6–C-*o* compared to Fe_1–N_4–C.

Our study delved into the coordination environment of dual-atomic Ni_2 centers in Ni_2 HDACs, emphasizing the resulted alteration of electron configurations on electrocatalytic CO_2 reduction.[16] Through the pyrolysis of a dinuclear nickel complex, $[Ni_2(L_1)_2(L_2)_2(H_2O)_2]\cdot 2H_2O$ (where L_1 represents adenine and H_2L_2 denotes malonic acid), alongside carbon black and dicyandiamide at temperatures of 700, 800, and 900 °C respectively, three distinct Ni_2 implanted N-doped carbon catalysts were synthesized, namely Ni_2-N_7, Ni_2-N_5C_2, and Ni_2-N_3C_4 (represented as Ni_2-N_xC_y; Figure 4a). Aberration corrected HAADF-STEM images of Ni_2-N_xC_y vividly revealed a preponderance of Ni atoms secured onto the N-doped carbon. Especially noteworthy were the conspicuous paired bright dots, which can be ascribed to dual-atomic Ni_2, spaced at an approximate distance of 3.1 Å (Figure 4b). The Ni K-edge XANES spectra further elucidated that all these catalysts have energy absorption thresholds situated between those of Ni foil and NiO, indicating that the Ni valence oscillates between 0 and +2. Sequentially, a discernible energy shift towards the higher end was observed for Ni_2-N_3C_4, Ni_2-N_5C_2, and Ni_2-N_7. The extended X-ray absorption fine structure (EXAFS) analysis corroborated that the dual-atomic Ni sites in Ni_2-N_3C_4 are bridged by a single N atom (Figure 4c). These configurations showcased an electronic structure that had been fine-tuned by varying the coordination environment around the dual-atomic Ni_2 center.

Significantly, the Ni_2-N_3C_4 configuration demonstrated exceptional electrocatalytic activity for CO_2 reduction, outperforming its single-atom Ni catalyst counterpart as well as other Ni_2 HDACs. At a potential of −0.60 V, the Ni_2-N_3C_4 achieved a current density of 151.26 mA cm^{-2} and a CO selectivity of 96.4%, underscoring its superior performance in electrocatalytic CO_2RR. Furthermore, Ni_2-N_3C_4 exhibited a higher current density than Ni_2-N_7 and Ni_2-N_5C_2, following the sequence of Ni_2-N_3C_4 > Ni_2-N_5C_2 > Ni_2-N_7 (Figure 5a). And the FE_{CO} of Ni_2-N_3C_4 consistently scored high across a potential range of −0.68 to −1.08 V, peaking at an impressive 98.9% at −0.88 V vs. RHE, a value that significantly surpassed that of Ni-N_2C_2 (Figure 5b).

DFT calculations offered deeper insights into the remarkably enhanced activity of Ni_2-N_3C_4 in electrocatalytic CO_2 reduction to CO. Within this structure, one Ni serves as the active site in CO_2RR, while the other contributes to the CO_2RR by refining the electronic structure of the active site, amplifying CO_2RR efficiency (Figure 5c). The high electrocatalytic activity of Ni_2-N_3C_4 for CO_2 reduction could be attributed to the electronic structure modulation to the Ni centre and the resulted proper binding energies to COOH* and CO* intermediates (Figure 5d). Thus, meticulous modulation of the coordination environment of the catalytic center in DACs can critically influence the electrocatalytic properties of DACs, with the Ni_2-N_3C_4 configuration emerging as a leading contender in the efficient CO_2RR.

Summary and Outlook

The concept underscores the pivotal role of homonuclear dual-atomic sites configurations in enhancing CO_2RR activity. Dual-atomic configurations present a promising avenue in the realm of electrocatalytic reduction of CO_2. However, challenges still persist. The synthesis of diatomic catalysts is intricate due to the intrinsic properties of substrate, which lead to unevenly dispersed diatomic sites. Addressing this requires innovations in spatial constraints, defect engineering, and metal-support coordination. Additionally, capturing the complex valence shifts of active sites during reactions is challenging, necessitating advanced in situ characterization techniques to unravel structure-activity nuances. Currently, the applications of diatomic catalysts in CO_2 reduction are limited mostly to C1 and C2 products. Incorporating elements like Cu, Sn, Bi, and Sb could

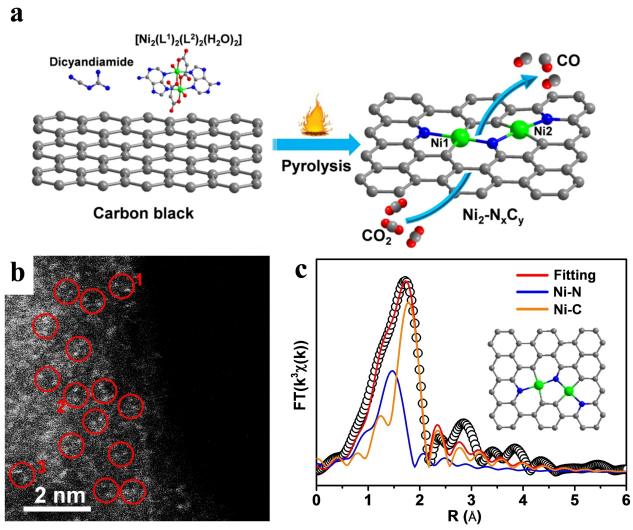

Figure 4. (a) Scheme of one-step pyrolysis strategy for the fabrication of Ni_2-N_xC_y catalysts for electrocatalytic CO_2 reduction to CO. (b) Aberration corrected HAADF-STEM image of Ni_2-N_3C_4. (c) EXAFS fittings and (inset) optimized models for Ni_2-N_3C_4. Reprinted with permission from Ref. [16] Copyright 2022, John Wiley and Sons.

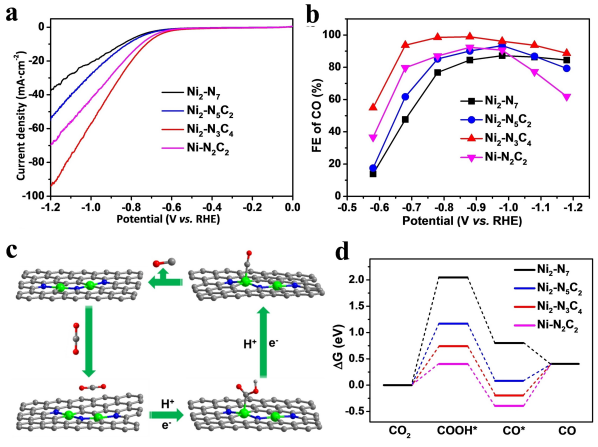

Figure 5. (a) LSV curves and (b) FEs of CO at different applied potentials for Ni_2-N_xC_y and Ni-N_2C_2 in the CO_2-saturated 0.5 M $KHCO_3$ electrolyte in the H-type cell. (c) Proposed reaction paths for the electroreduction of CO_2 to CO over Ni_2-N_3C_4. (d) Free energy profiles of the electroreduction of CO_2 to CO of Ni sites for Ni_2-N_xC_y and Ni-N_2C_2. Reprinted with permission from Ref. [16] Copyright 2022, John Wiley and Sons.

diversify hydrocarbon product outputs. Through precise atomic modulation and electronic interactions, not only can the reduction process of CO_2 be optimized, but invaluable insights can also be provided for future electrocatalytic applications. To achieve more efficient and sustainable CO_2 transformations, future endeavors should further explore and refine these configurations.

Acknowledgements

This work was supported by the National Key R&D Program of China (2022YFA1502902), the National Natural Science Foundation of China (22271218, 22071182, 22201209, and 21931007).

Conflict of Interests

The authors declare no conflict of interest.

Data Availability Statement

Data sharing is not applicable to this article as no new data were created or analyzed in this study.

Keywords: CO_2 reduction · electrocatalytic · electronic modulation · homonuclear dual-atomic catalysts · synergistic effect

[1] a) D. Liu, D. Zhong, T. Lu, *EnergyChem* **2020**, *2*, 100034; b) S. Solomon, G.-K. Plattner, R. Knutti, P. Friedlingstein, *Proc. Nat. Acad. Sci.* **2009**, *106*, 1704–1709; c) Y. Zhou, J. Zhang, L. Wang, X. Cui, X. Liu, S. S. Wong, H. An, N. Yan, J. Xie, C. Yu, C Yu, P Zhang, Y Du, S Xi, L Zheng, X. Cao, Y. Wu, Y. Wang, C. Wang, H. Wen, L. Chen, H. Xing, J. Wang, *Science* **2021**, *373*, 315–320.

[2] a) J. Resasco, A. T. Bell, *Trends Chem.* **2020**, *2*, 825–836; b) C. Wang, Z. Lv, W. Yang, X. Feng, B. Wang, *Chem. Soc. Rev.* **2023**, *52*, 1382–1427; c) Z. Zhang, X. Huang, Z. Chen, J. Zhu, B. Endrődi, C. Janáky, D. Deng, *Angew. Chem. Int. Ed.* **2023**, *62*, e202302789.

[3] a) N. Cheng, L. Zhang, K. Doyle-Davis, X. Sun, *Electrochem. Energy Rev.* **2019**, *2*, 539–573; b) M. B. Gawande, P. Fornasiero, R. Zbořil, *ACS Catal.* **2020**, *10*, 2231–2259; c) J. Yang, W. Li, D. Wang, Y. Li, *Adv. Mater.* **2020**, *32*, 2003300; d) X.-F. Yang, A. Wang, B. Qiao, J. Li, J. Liu, T. Zhang, *Acc. Chem. Res.* **2013**, *46*, 1740–1748.

[4] a) R. Li, D. Wang, *Adv. Energy Mater.* **2022**, *12*, 2103564; b) J. Zhang, Q.-a. Huang, J. Wang, J. Wang, J. Zhang, Y. Zhao, *Chin. J. Catal.* **2020**, *41*, 783–798; c) W. Zhang, Y. Chao, W. Zhang, J. Zhou, F. Lv, K. Wang, F. Lin, H. Luo, J. Li, M. Tong, E. Wang, S. Guo, *Adv. Mater.* **2021**, *33*, 2102576.

[5] a) Y. Li, H. Su, S. H. Chan, Q. Sun, *ACS Catal.* **2015**, *5*, 6658–6664; b) Z. Liang, L. Song, M. Sun, B. Huang, Y. Du, *Sci. Adv.*, *7*, eabl4915.

[6] a) J. Linnemann, K. Kanokkanchana, K. Tschulik, *ACS Catal.* **2021**, *11*, 5318–5346; b) H. Yang, Y. Chen, Y. Qin, *Chin. J. Catal.* **2020**, *41*, 227–241.

[7] a) S. Cao, S. Wei, X. Wei, S. Zhou, H. Chen, Y. Hu, Z. Wang, S. Liu, W. Guo, X. Lu, *Small* **2021**, *17*, 2100949; b) M. Li, H. Wang, W. Luo, P. C. Sherrell, J. Chen, J. Yang, *Adv. Mater.* **2020**, *32*, 2001848; c) M. Ma, F. Li, Q. Tang, *Nanoscale* **2021**, *13*, 19133–19143; d) Y. Shao, Q. Yuan, J. Zhou, *Small* **2023**, *19*, 2303446; e) Z. Zhang, J. Zhu, S. Chen, W. Sun, D. Wang, *Angew. Chem. Int. Ed.* **2023**, *62*, e202215136.

[8] N. Qiu, J. Li, H. Wang, Z. Zhang, *Sci. China Mater.* **2022**, *65*, 3302–3323.

[9] a) M. He, W. An, Y. Wang, Y. Men, S. Liu, *Small* **2021**, *17*, 2104445; b) M. Jafarzadeh, K. Daasbjerg, *ACS Appl. Energ. Mater.* **2023**, *6*, 6851–6882.

[10] a) T. Tang, Z. Wang, J. Guan, *Coord. Chem. Rev.* **2023**, *492*, 215288; b) J. Wang, C. Liu, S. Li, Y. Li, Q. Zhang, Q. Peng, J. S. Tse, Z. Wu, *Chem. Eng. J.* **2022**, *428*, 132558.

[11] N. Zhang, X. Zhang, Y. Kang, C. Ye, R. Jin, H. Yan, R. Lin, J. Yang, Q. Xu, Y. Wang, Q. Zhang, L. Gu, L. Liu, W. Song, J. Liu, D. Wang, Y. Li, *Angew. Chem. Int. Ed.* **2021**, *60*, 13388–13393.

[12] T. Ding, X. Liu, Z. Tao, T. Liu, T. Chen, W. Zhang, X. Shen, D. Liu, S. Wang, B. Pang, D. Wu, L. Cao, L. Wang, T. Liu, Y. Li, H. Sheng, M. Zhu, T. Yao, *J. Am. Chem. Soc.* **2021**, *143*, 11317–11324.

[13] Y. Zhu, J. Sokolowski, X. Song, Y. He, Y. Mei, G. Wu, *Adv. Energy Mater.* **2020**, *10*, 1902844.

[14] J. Gu, C. S. Hsu, L. Bai, H. M. Chen, X. Hu, *Science* **2019**, *364*, 1091–1094.

[15] Y. Wang, B. J. Park, V. K. Paidi, R. Huang, Y. Lee, K.-J. Noh, K.-S. Lee, J. W. Han, *ACS Energy Lett.* **2022**, *7*, 640–649.

[16] Y. Gong, C. Cao, W. Shi, J. Zhang, J. Deng, T. Lu, D. Zhong, *Angew. Chem. Int. Ed.* **2022**, *61*, e202215187.

Manuscript received: October 11, 2023
Accepted manuscript online: November 14, 2023
Version of record online: November 30, 2023